Aqueous Suspensions of Natural Swelling Clay Minerals. 2. Rheological Characterization

ARTICLE *in* LANGMUIR · JUNE 2011

Impact Factor: 4.46 · DOI: 10.1021/la2001267 · Source: PubMed

4 AUTHORS, INCLUDING:

Erwan Paineau
French National Centre for Scientific Research
31 PUBLICATIONS **314** CITATIONS
SEE PROFILE

Laurent J Michot
French National Centre for Scientific Research
160 PUBLICATIONS **3,283** CITATIONS
SEE PROFILE

Isabelle Bihannic
French National Centre for Scientific Research
50 PUBLICATIONS **996** CITATIONS
SEE PROFILE

Langmuir

ARTICLE

pubs.acs.org/Langmuir

Aqueous Suspensions of Natural Swelling Clay Minerals. 2. Rheological Characterization

Erwan Paineau,*[,†] Laurent J. Michot,[†] Isabelle Bihannic,[†] and Christophe Baravian*[,‡]

[†]Laboratoire Environnement et Minéralurgie, Nancy University CNRS-INPL, UMR 7569, BP40 54501 Vandœuvre, Cedex France

[‡]Laboratoire d'Energétique et de Mécanique Théorique et Appliquée, Nancy University, UMR 7563, CNRS-INPL-UHP, 2 Avenue de la Forêt de Haye, BP160 54504 Vandœuvre, Cedex, France

Supporting Information

ABSTRACT: We report in this article a comprehensive investigation of the viscoelastic behavior of different natural colloidal clay minerals in aqueous solution. Rheological experiments were carried out under both dynamic and steady-state conditions, allowing us to derive the elasticity and yield stress. Both parameters can be renormalized for all sizes, ionic strength, and type of clay using in a first approach only the volume of the particles. However, applying such a treatment to various clays of similar shapes and sizes yields differences that can be linked to the repulsion strength and charge location in the swelling clays. The stronger the repulsive interactions, the better the orientation of clay particles in flows. In addition, a master linear relationship between the elasticity and yield stress whose value corresponds to a critical deformation of 0.1 was evidenced. Such a relationship may be general for any colloidal suspension of anisometric particles as revealed by the analysis of various experimental data obtained on either disk-shaped or lath- and rod-shaped particles. The particle size dependence of the sol−gel transition was also investigated in detail. To understand why suspensions of larger particles gel at a higher volume fraction, we propose a very simplified view based on the statistical hydrodynamic trapping of a particle by an another one in its neighborhood upon translation and during a short period of time. We show that the key parameter describing this hydrodynamic trapping varies as the cube of the average diameter and captures most features of the sol−gel transition. Finally, we pointed out that in the high shear limit the suspension viscosity is still closely related to electrostatic interactions and follows the same trends as the viscoelastic properties.

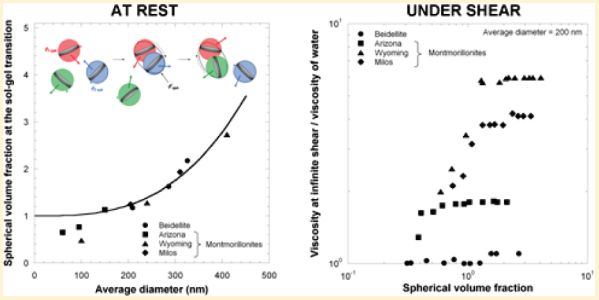

INTRODUCTION

Swelling clay minerals are fascinating materials that are widespread on the earth's surface and have been intensively used since the Neolithic period.[1] These natural minerals are 2:1 layered aluminosilicate compounds composed of two tetrahedral sheets encompassing an octahedral one. Isomorphous substitutions occur in both layers, inducing a charge deficit compensated by interlayer exchangeable cations. When dispersed in water, clay minerals present a wide range of colloidal behavior (thixotropy, viscoelasticity, and yield stress) that differs with the chemical composition, size, and shape of the clay used. It is also highly dependent on the nature of the exchangeable cation. These features, involved in various commercial and industrial applications (drilling fluids in the oil industry, nanofillers in paint and plastic products ,or additives in the food, cosmetic, and pharmaceutical industries)[2,3] have been intensively studied since 1928 when Freundlich first reported on the thixotropic behavior of gels[4] of Wyoming bentonite, a rock mainly composed of montmorillonite.[5] A few years later, Broughton and Squires investigated the effects of clay concentration on the gelation of centrifuged Wyoming dispersions.[6] They interpreted their viscosity measurements in the gel as corresponding to the formation of a 3D network where clay particles are randomly oriented with edge−edge contacts. Hauser and Reed[7] analyzed the effect of particle size on the thixotropy of Wyoming bentonite. They favored a repulsive model and showed that reducing the average size induced the gelation of clay suspensions at lower concentrations. The birefringence relaxation of similar gelified systems was investigated by Langmuir,[8] thus revealing the alignment of the particles in the flow. Since this pioneering work, the structure of the gel and the mechanism of gelation have remained unclear and two conflicting modes of interaction between clay particles have been opposed. (i) Van Olphen suggested the formation of a 3D "house of cards" network that may occur through face−face (FF), edge−edge (EE), or edge−face (EF) associations.[9,10] According to such an assumption, EF interactions induced by electrostatic attractions between the opposite charges of the edges (+) and faces (−) should dominate under acidic conditions,[11,12] a feature that has been confirmed by various rheological measurements.[6,13−21] Still, several authors alternatively described gelation either as the EE clay orientation in the form of "zig-zag" flat ribbons[22,23] or as a combination of EE and FF coagulation[24−27] forming bandlike structures.[28] According to Brandenburg and Lagaly, both types of

Received: January 11, 2011
Revised: May 3, 2011
Published: May 18, 2011

Table 1. Chemical Formulae of the Studied Clays

clay	origin	composition
SBId-1	Idaho	$(Si_{7.27}Al_{0.73})(Al_{3.77}Fe^{3+}_{0.11}Mg_{0.21})O_{20}(OH)_4Na_{0.67}$
SAz-1	Arizona	$(Si_{7.95}Al_{0.05})(Al_{2.75}Fe^{3+}_{0.17}Mg_{1.07})O_{20}(OH)_4Na_{1.11}$
SWy-2	Wyoming	$(Si_{7.74}Al_{0.26})(Al_{3.06}Fe^{3+}_{0.42}Fe^{2+}_{0.03}Mg_{0.48})O_{20}(OH)_4Na_{0.77}$
Mil	Milos	$(Si_{7.76}Al_{0.24})(Al_3Fe^{3+}_{0.44}Fe^{2+}_{0.02}Mg_{0.54})O_{20}(OH)_4Na_{0.79}$

Table 2. Morphological Parameters of the Studied Clays[a]

name	SBId-1			SAz-1				SWy-2				Milos			
size	S1	S2	S3	S1	S2	S3	S4	S1	S2	S3	S4	S1	S2	S3	S4
average diameter (nm)	326	286	209	295	150	95	***60***	410	240	100	***40***	310	205	140	100
polydispersity diameter (%)	47	45	38	90	42	19	***nd***	170	93	25	***nd***	80	41	17	8
average thickness (nm)	1.1	0.85	0.7	1	0.8	0.75	0.65	1	0.7	0.7	0.65	1.05	0.75	0.7	0.7

[a] Bold characters correspond to estimated values. nd: not determined.

Table 3. Experimental Procedure of the Rheological Measurements

stage	step	parameters
1	resting	set T = 25 °C
		t = 3 min
2	oscillation frequency sweep (I)	τ controlled
		ν = 0.02 to 10 Hz
3	preshearing	$\dot{\gamma}$ = 5000 s^{-1}
		t = 1 min
4	resting	set T = 25 °C
		t = 3 min
5	ascending flow curve	$\dot{\gamma}$= 0.1 to 5000 s^{-1}
		t = 10 s/pt
6	descending flow curve	$\dot{\gamma}$= 5000 to 0.1 s^{-1}
		t = 10 s/pt
7	oscillation frequency sweep (II)	τ controlled
		ν = 0.1 to 10 Hz
8	oscillation amplitude sweep	ν controlled (1 Hz)
		τ = 0.05 to 500 Pa

structures can exist because they interpreted their rheological curves as indicating a continuous transition from a card-house network to a bandlike structure upon the addition of calcium ions with increasing pH.[29,30] (ii) A completely different view was proposed by Hauser[31] and Norrish[32] according to whom the gel structure is stabilized by repulsive forces between the interacting electrical double layers of the platelets. Such an interpretation is strongly supported by the measurement of interparticle forces[33,34] and rheological properties.[35−44] Various scattering (light, X-ray, and neutron) and NMR experiments have also been performed and were briefly reviewed in our previous publication.[45] Most of these studies were performed at neutral pH,[31−44] and several additional studies presented pH-dependent models combining both attractive and repulsive mechanisms.[46−52] The occurrence of fractal[53−55] or cluster[56,57] associations was also suggested as a possible mechanism explaining the macroscopic structure of the gel. This brief review of the literature data clearly shows that gelation mechanisms of swelling clay minerals are still far from being clearly understood. To try to clarify the situation, it is crucial to work on well-characterized mineralogical species and to use size-selected samples at constant ionic strength. Indeed, as shown by various studies, crystal chemistry parameters and notably the location in the structure of charge deficit have a significant influence on the phase behavior of swelling clay minerals. Indeed, numerous tetrahedrally substituted clay minerals such as nontronites[43,44,58,59] and beidellite[60] present a true isotropic/nematic liquid-crystal phase transition before the sol−gel transition. In contrast, in most octahedrally substituted clays, only a sol−gel transition is observed. It must be pointed out, however, that fluorohectorite,[61,62] which belongs to this latter subgroup, has recently been shown to present an isotropic/nematic transition that involves stacks of platelets and not individual layers. Although additional experimental and simulation work is clearly required, these features could be tentatively assigned to subtle changes in ionic repulsions, where tetrahedrally substituted clays could be more repulsive than octahedral ones, a conclusion supported, for the samples we studied, by changes in the suspension structure presented in the first part of this series of papers.[45] The aim of this article is to analyze in depth for the same samples the static and dynamic rheological behavior of aqueous suspensions to assess the influence of changes in repulsion on the mechanical properties. This analysis will be limited to ionic strengths lower than 10^{-3} mol/L (i.e., in a range where the system can be considered to be purely repulsive[45]). The role of particle anisometry in the rheological behavior,[63,64] particularly on the sol−gel transition that was shown to depend on the average size,[41,43,44] will be investigated by using size-selected particles.

MATERIALS AND METHODS

Four natural dioctahedral smectites, one beidellite (SBId-1, Idaho) and three montmorillonites (SAz-1, Arizona; SWy-2, Wyoming; Mil, Milos, Greece), were purchased from the Source Clays Minerals Repository of the Clay Mineral Society (Purdue University), except for the Milos clay that was kindly supplied by Iko Erbslöh (Germany). All clays belong to the montmorillonite-beidellite series[65] according to the structural formula $[Si_{8-x}Al_x][Al_{4-y}(Fe, Mg)_y]O_{20}(OH)_4Na^+_{x+y}, nH_2O$. The chemical formulas of these four samples, deduced from the chemical analyses,[60,66] are summarized in Table 1.

Before use, natural clay samples were purified following the procedure established previously.[60] After the raw sample was ground, a 40 $g \cdot L^{-1}$ clay suspension was exchanged three times in 1 M NaCl solution over a period of 24 h. Excess chloride was then removed by dialyzing the suspension against Milli-Q water until the conductivity was below

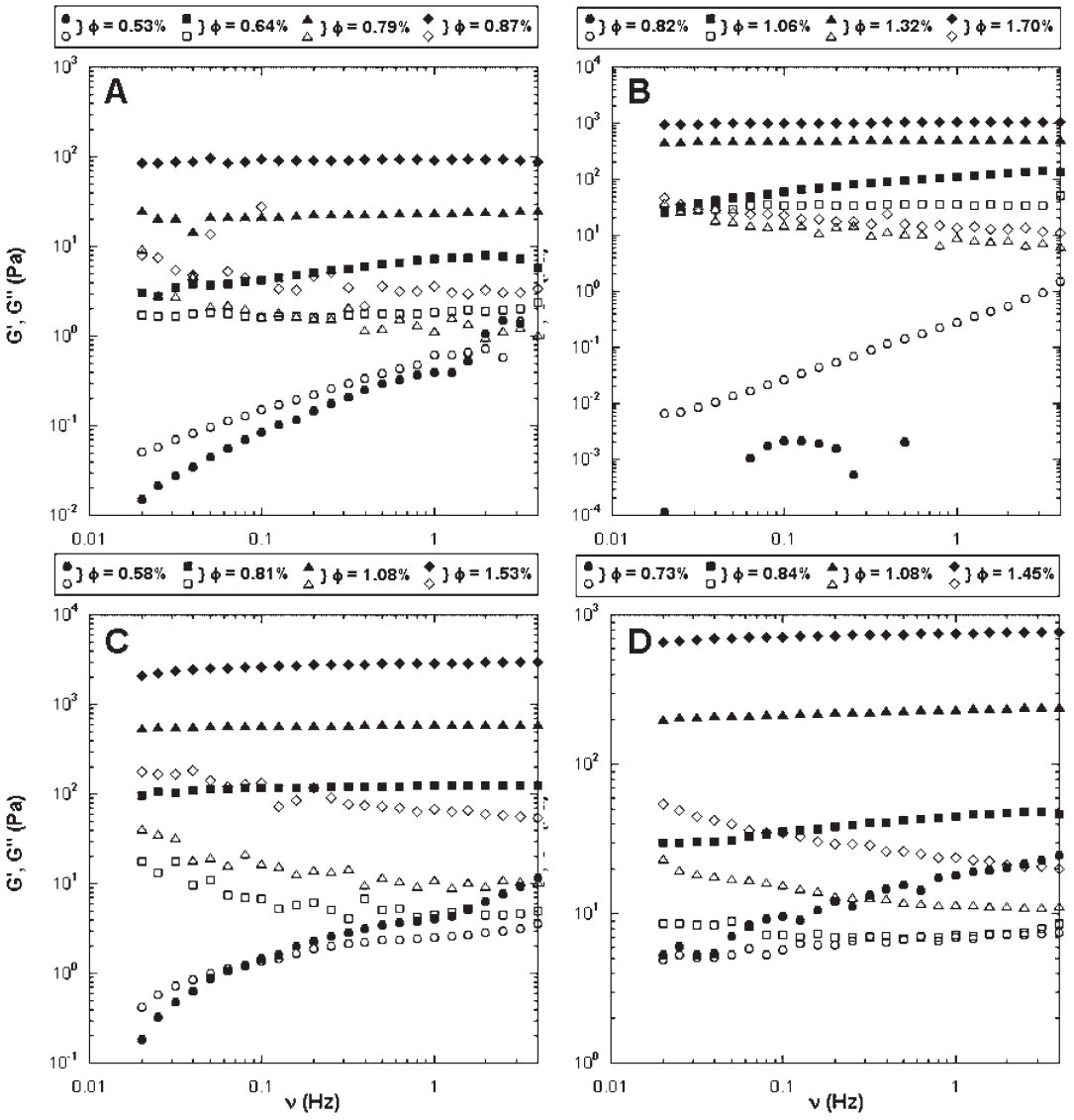

Figure 1. Evolution of the elastic (G', filled symbols) and viscous (G'', open symbols) moduli with oscillation frequency for the different smectite aqueous suspensions at an ionic strength of 10^{-5} M·L^{-1}. (A) SBId-1 S3, (B) SAz-1 S2, (C) SWy-2 S2, and (D) Milos S2.

5 μS·m^{-1}. After recovery from the dialysis tubes, the suspension was then transferred to Imhoff cones and was left to sediment for 24 h. The supernatant was then siphoned off because the bottom of the cone contains miscellaneous impurities (mainly sand-size quartz, feldspar, and oxyhydroxydes) that were discarded. To reduce the polydispersity, a size fractionation procedure was then applied by successive centrifugation. The stock suspension was first centrifuged at 7000*g* for 90 min. The sediment was collected and rediluted in Milli-Q water and will be referred to as size 1 (S1) hereafter. The same procedure was then applied after centrifugation at 17000*g* and 35000*g*, thus yielding size 2 (S2) and size 3 (S3) fractions. The final supernatant was concentrated by rotaevaporation and will correspond to size 4 (S4), except for beidellite that has only three size fractions.[45] The elementary particles of all of these aluminous dioctahedral smectites display disklike morphology. The morphological parameters of all size fractions determined by transmission electron microscopy (TEM) and small angle X-ray scattering (SAXS) experiments[45] are reported in Table 2. Deducing the thickness from swelling laws obtained by SAXS has the advantage of providing self-consistent values. It must be pointed out, however, that such a procedure does not allow us to account for the possible structural heterogeneity linked to the use of natural samples. All experimental details have been published elsewhere.[60]

Osmotic stress experiments were performed at a fixed ionic strength (IS = 10^{-5}, 10^{-4}, and 10^{-3} M·L^{-1}) to obtain a wide concentration range of clay suspensions varying from the liquid to the gel phase. Regenerated cellulose dialysis tubes (Visking, MWCO = 14000 Da, Roth) were filled with clay suspensions and put into a poly(ethylene glycol) solution (PEG 20000, Roth) whose ionic strength is adjusted with NaCl. Sample preparations are detailed elsewhere.[60] The clay volume fraction ϕ is then determined by weight loss upon drying.

Rheological measurements were performed at 25 °C on a controlled-stress Aspect rheometer 2000 (TA Instruments) with a small cone and plate geometry with a diameter of 20 mm, a gap of 14 μm, and an angle of 0.30°, allowing us to reach high shear rates $\dot{\gamma}$ during the flow steps. To prevent any sample drying, the geometry was equipped with an antievaporation device.

The rheological sequence, summarized in Table 3, starts with a preshearing stage (1 min, $\dot{\gamma}$ = 5000 s^{-1}) to avoid artifacts due to sample

dx.doi.org/10.1021/la2001267 |*Langmuir* 2011, 27, 7806–7819

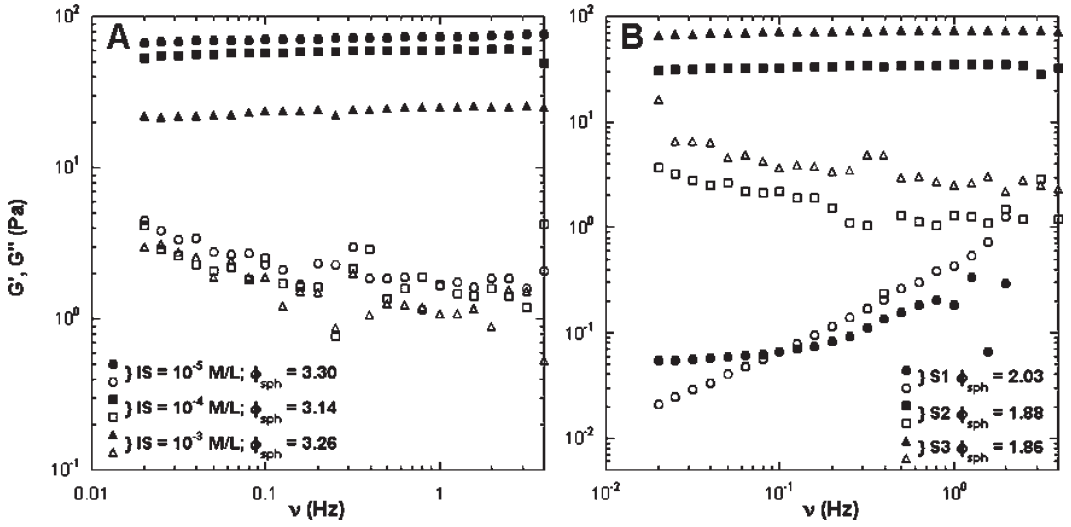

Figure 2. Evolution of the elastic (G', filled symbols) and viscous (G'', open symbols) moduli with oscillation frequency for various beidellite suspensions of equivalent spherical volume fractions ϕ_{sph}. (A) Influence of the ionic strength (SBId-1 S2). (B) Influence of the particle size (IS = 10^{-4} M·L^{-1}).

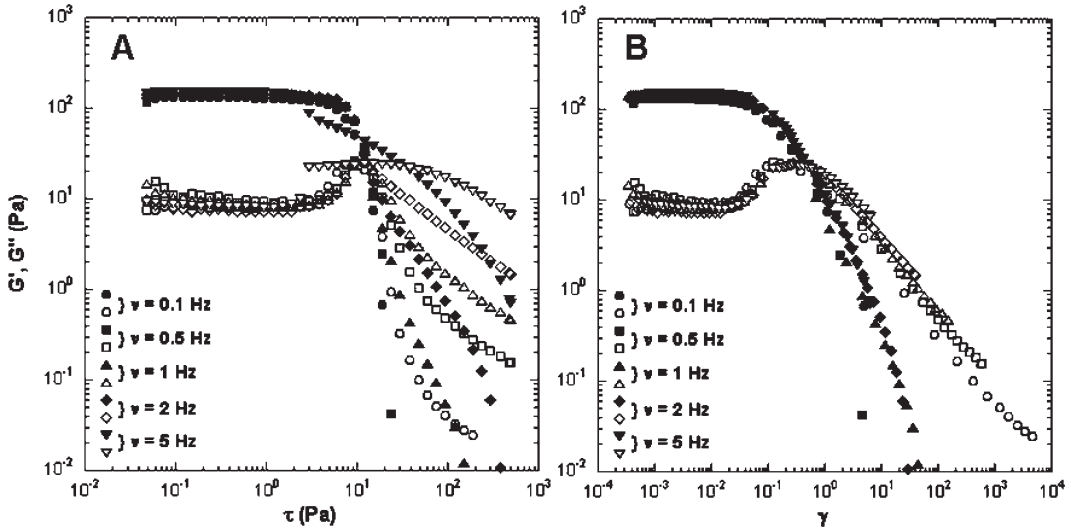

Figure 3. Typical variations of the elastic (G', filled symbols) and viscous (G'', open symbols) modulus with (A) oscillation stress or (B) strain at different imposed oscillation frequencies for a size 2 Wyoming suspension (IS = 10^{-5} M·L^{-1}; ϕ = 0.91%).

positioning. Steady-state flow curves are then recorded under a controlled shear rate from 0 to 5000 s^{-1} in one cycle of increasing and decreasing shear rates with a logarithmic step (10 points per decade). In all cases, upward and downward ramps are superimposed, which shows that a steady state is actually measured. The material is then definitely not thixotropic over the timescale of the present study. After this cycle, the elastic G' and viscous G'' moduli were measured again in an oscillation frequency sweep using frequencies ν of between 0.02 and 10 Hz. Performing oscillation sweeps before and after steady-flow curves allows us to control for the presence of potential irreversible changes due to the flow curves, which was never observed. The strain γ used in the oscillatory measurements was chosen in the linear viscoelastic regime (LVR). Finally, after the second oscillatory stress, an oscillation amplitude sweep at a fixed frequency of 1 Hz (discussed below) was performed using an oscillation stress τ of between 0.05 and 500 Pa corresponding to an applied strain γ of between 2 × 10^{-5} and 40.

RESULTS

For clarity, not all experimental curves are represented. As shown in Table 2, all clays display a common size fraction with a mean diameter close to 200 nm (beidellite, S3; montmorillonites, S2). Thus, in the following text, all presented curves will concern Na-smectite suspensions with this common particle size, except when studying the effect of either ionic strength or size.

Dynamic Rheological Measurements. *Oscillation Frequency Sweep.* The frequency dependences of both elastic G' and viscous G'' moduli at an ionic strength of 10^{-5} M·L^{-1} are presented in Figure 1.

Both beidellite and montmorillonites present similar evolutions with increasing concentration. For the higher volume fractions, G' is much higher than G'' and exhibits a limited frequency dependence, a feature typical of a gel.[41,43,67] The

dx.doi.org/10.1021/la2001267 |*Langmuir* 2011, 27, 7806–7819

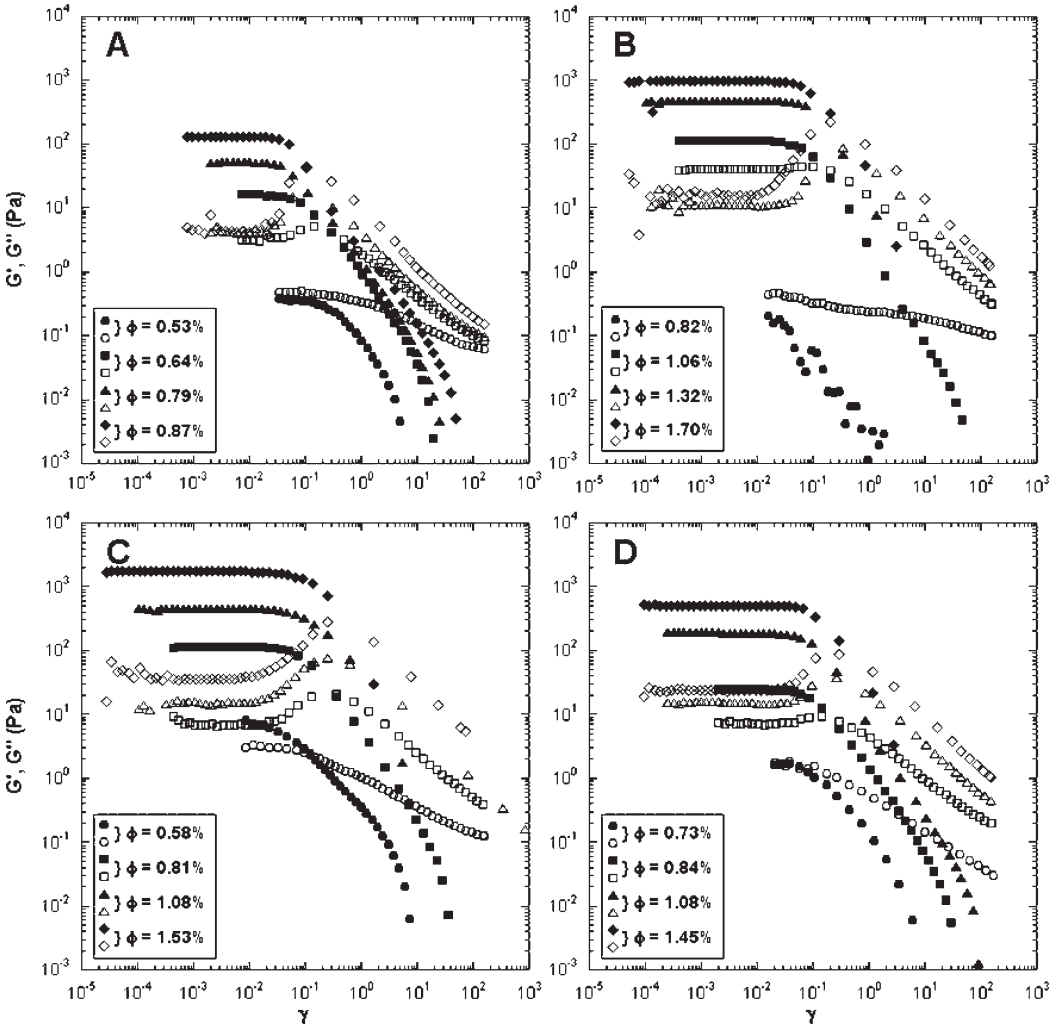

Figure 4. Evolution of the elastic (G', filled symbols) and viscous (G'', open symbols) moduli with strain for the different smectite aqueous suspensions at an ionic strength of 10^{-5} M·L^{-1}. (A) SBId-1 S3, (B) SAz-1 S2, (C) SWy-2 S2, and (D) Milos S2.

variations (not shown) above 5 Hz are due to inertial effects of the rheometer.[68] At low volume fractions, G' and G'' are of the same order of magnitude and display a frequency dependence corresponding to viscoelastic liquids (Figure 1). The critical volume fraction corresponding to the transition between these two domains seems to be lower for beidellite than for montmorillonites. It can also be pointed out that for the lowest concentrations both moduli present a frequency dependence scaling as $G' \approx \omega^2$ and $G'' \approx \omega$, typical of Maxwellian behavior (data shown in Supporting Information, Figure S1).

The ionic strength and particle size can drastically affect the viscoelasticity of clay suspensions.[39,41,43] This is presented in Figure 2 in the case of beidellite suspensions with equivalent spherical volume fractions ϕ_{sph} defined as the volume fraction of spheres encompassing the clay particles that, for disks, can be written as[69]

$$\phi_{sph} = \frac{2}{3}\frac{\langle D \rangle}{t}\phi \qquad (1)$$

For each clay sample, the correspondence between the true volume fraction and the equivalent spherical volume fractions ϕ_{sph} can be simply obtained from the morphological parameters reported in Table 2. As already shown,[40,43−45,69] the use of ϕ_{sph} allows an easy comparison between various samples and captures the main features linked to size effects.

For equivalent spherical volume fractions, an increase in ionic strength (up to 10^{-3} M·L^{-1}) or in particle size shifts the values of both G' and G'' toward lower values. The influence of particle size is particularly significant. Indeed, an increase in the average size of beidellite by a factor of 1.5 induces a sharp decrease in G' (Figure 2B), a feature already observed in nontronites suspensions.[43,44]

Oscillation Amplitude Sweep. Oscillation amplitude sweeps were carried out for five applied frequencies varying from 0.1 to 5 Hz. As an illustration, Figure 3 presents the results obtained on a gel sample of SWy-2 (ϕ = 0.91%) at an ionic strength of 10^{-5} M·L^{-1}.

Whatever the frequency used, the curves are all superimposed in the LVR for stresses lower than 1 Pa (Figure 3A). When plotted as a function of strain (Figure 3B), such superimposition extends to the whole strain range. Similar results have been obtained for gelified samples of beidellite, Milos, and Arizona montmorillonites. All subsequent amplitude sweep experiments were then carried out at a fixed frequency of 1 Hz

Figure 4 displays the evolution with oscillation strains of G' and G'' for beidellite and montmorillonites at various volume

dx.doi.org/10.1021/la2001267 |*Langmuir* 2011, 27, 7806–7819

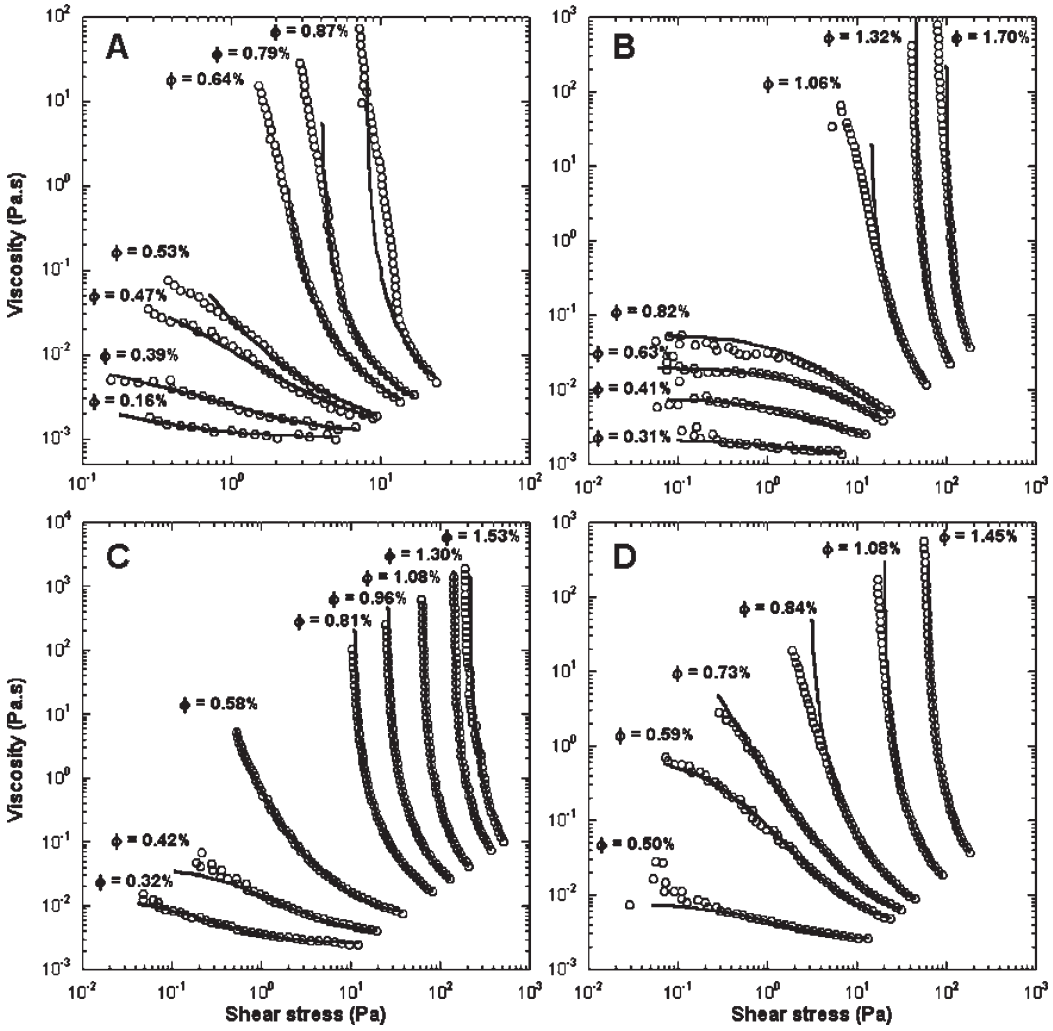

Figure 5. Flow curves (viscosity vs shear stress) of the different smectite aqueous suspensions at an ionic strength of 10^{-5} M·L^{-1}. The solid black line corresponds to the adjustment of eq 3. (A) SBId-1 S3, (B) SAz-1 S2, (C) SWy-2 S2, and (D) Milos S2.

fractions. The same data plotted as a function of oscillation stress are presented in Figure S2 in the Supporting Information. The curves are rather similar whatever the clay used, and all decrease for a critical strain value of close to 0.1. This clearly shows that the breaking of the material is controlled by a critical deformation.[35,42,70−73]

Steady-State Flow Curves. Although oscillatory experiments provide a quick way to determine the volume fraction at the sol−gel transition, such measurements can underestimate the real volume fraction of the sol−gel transition. To derive a relevant physical interpretation of the flow curves, we have chosen to use the model proposed by Quemada and co-workers[74−76] based on the definition of an effective hydrodynamic volume fraction. Such an approach has indeed proven efficient for interpreting the rheological behavior of numerous colloidal systems and, as shown by Baravian et al.,[40] can be extended to the case of anisometric particles. A hydrodynamic Peclet number that compares shear effects to interaction energy E is derived. In a dilute suspension where interactions between particles are negligible, E is equal to kT (i.e., the thermal Brownian energy)

$$Pe \approx \frac{\sigma {r_{eq}}^3}{E} \equiv \frac{\sigma}{\sigma_c} \qquad (2)$$

where $\sigma {r_{eq}}^3$ represents the hydrodynamic energy, σ represents the shear stress, r_{eq} represents the average disk radius, and σ_c represents the critical shear stress. Hydrodynamic effects are comparable to Brownian and interaction energies when the shear stress reaches this critical threshold. Viscosity measurements under shear stress can then be fitted using an extended hard-sphere model[40,43]

$$\eta_r = \frac{\eta_\infty}{\eta_f}\left(\frac{1+Pe}{\chi+Pe}\right)^2 \text{ with } \chi = \frac{1-\frac{\alpha\phi_{sph}}{\phi_0^*}}{1-\frac{\alpha\phi_{sph}}{\phi_\infty^*}} \text{ and } (-1 \le \chi \le 1) \qquad (3)$$

where η_r is defined as the relative viscosity of the suspension, η_∞ is its viscosity under infinite shear, η_f is the viscosity of the suspending fluid, and ϕ_0^* and ϕ_∞^* are the critical packing fractions at rest ($Pe = 0$) and under infinite shear ($Pe \rightarrow \infty$), respectively. At low concentration, particles are free to rotate and therefore $\alpha = 1$. For increasing volume fraction or under shear, orientational effects must be taken into account by decreasing the value of α. In the limit of total orientation, $\alpha = 2t/\langle D \rangle$. Thus, if the viscosity remains

dx.doi.org/10.1021/la2001267 |*Langmuir* 2011, 27, 7806–7819

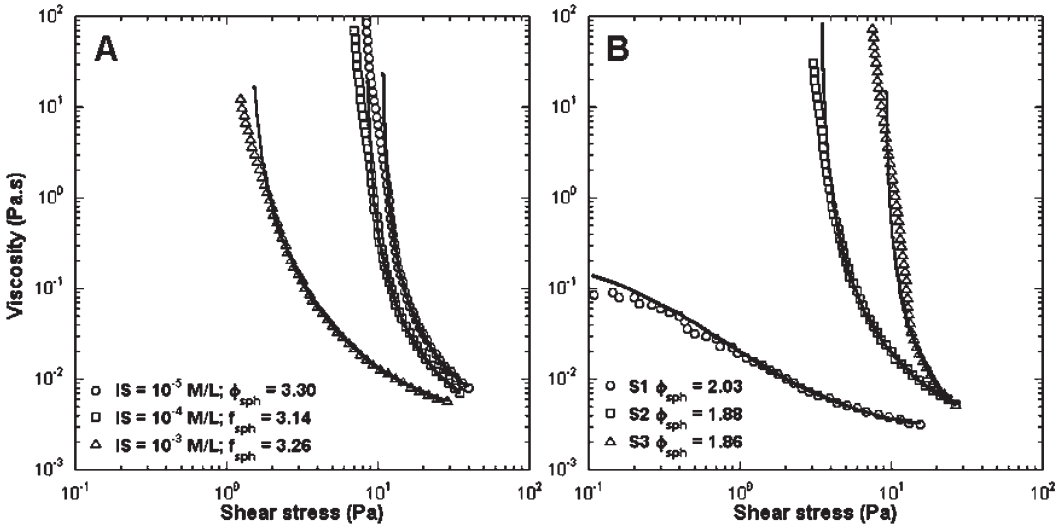

Figure 6. Influence of (A) ionic strength (SBId-1 S2) and (B) particle size (IS = 10^{-4} M·L^{-1}) on the flow curves of various beidellite suspensions of equivalent spherical volume fractions ϕ_{sph}. The solid black line corresponds to the adjustment of eq 3.

Table 4. Spherical Volume Fraction Corresponding to the Sol−Gel Transition of Various Smectite Suspensions Determined from Equation 3 for Various Ionic Strengths

name	SBId-1			SAz-1			SWy-2			Milos	
Size	S1	S2	S3	S2	S3	S4	S1	S2	S3	S1	S2
IS = 10^{-3} M/L	3.3	2.28	1.34	1							1.38
IS = 10^{-4} M/L	2.65	1.75	1.23	1.25			2.87	1.49		2.36	1.28
IS = 10^{-5} M/L	2.17	1.62	1.17	1.13	0.76	0.65	2.73	1.28	0.48	1.93	1.24

finite at rest, then χ is equal to

$$\chi = \left(\frac{\eta_\infty}{\eta_0}\right)^{1/2} \quad (4)$$

χ becomes negative when a yield stress σ_y appears at zero shear. The yield stress can then be derived as

$$\chi = -\frac{\sigma_y}{\sigma_c} \quad (5)$$

Hence, the sign inversion of the χ parameter corresponds to the effective volume fraction at which the suspension becomes a gel. Finally, using such a model, the flow curves (viscosity vs shear stress) can be fitted by three parameters, η_∞, χ, and σ_c. Figure 5 illustrates adjustment of eq 3 to the flow curves of beidellite and montmorillonites at an ionic strength of 10^{-5} M·L^{-1}.

The shape of the curves evolves with increasing volume fraction. At very dilute concentration, flow curves display Newtonian behavior close to the viscosity of water. With increasing volume fraction, the curves exhibit a Newtonian plateau at low and high shear stress, separated by a shear-thinning region (Figure 5B). Above a critical volume fraction, the viscosity at rest is no longer observed and the flow curves present an apparent yield stress σ_y. In most cases, the experimental curves are fully reproduced by the viscosity model except for curves with double inflections (Figure 7A, ϕ = 0.87%). Such a feature can be tentatively assigned to the motion of large structures in the geometry gap. In such a case, the intermediate regime cannot be modeled. For the smallest size fractions,[58] Pe is never significantly higher than 1. Therefore, for the highest investigated shear rates, the viscosity does not display any clear inflection, which makes the determination of η_∞ less accurate.

An increase in either the ionic strength or average particle size induces a decrease in the yield stress as shown in Figure 6.

Table 4 displays the spherical volume fractions corresponding to the sol−gel transition as derived from the change of sign of χ derived from the modeling procedure, where χ = 0.

As observed earlier for SWy-2 montmorillonite[41] and nontronites,[43,44] the smallest particles gel earlier than the larger ones. A tentative explanation of this nontrivial behavior will be discussed further.

Relation between Dynamic and Steady-State Rheological Measurements. Figure 7A presents the evolution of both dynamic and flow curves obtained for a concentrated sample of SWy-2 montmorillonite (ϕ_{sph} = 4.07)

In the linear viscoelastic regime, the gel sample displays an elastic response to the applied (oscillation or shear) stress. No deformation occurs until a critical stress is reached. At this point, the drop in the elastic modulus G' and the maximum in the viscous modulus G'' are well correlated with the onset of flow. To further illustrate such a feature, Figure 7B presents the evolution of the critical oscillation stress corresponding to the maximum of G'', $\tau_{G''\rightarrow max}$, as a function of the yield stress σ_y obtained from eq 5. A linear relationship between both parameters that is independent of the size volume fraction and clay type is obtained. This confirms the consistency of the results obtained by both dynamic and steady-state rheological measurements in defining the yield stress.

DISCUSSION

Elasticity Yield Stress. Figure 8 presents the evolution of the normalized elasticity and yield stress as a function of the spherical volume fraction for different size fractions of beidellite and montmorillonites at various ionic strengths. To normalize the results according to the Peclet number, G' and σ_y have both been multiplied by the volume of the sphere encompassing the disk

dx.doi.org/10.1021/la2001267 |Langmuir 2011, 27, 7806–7819

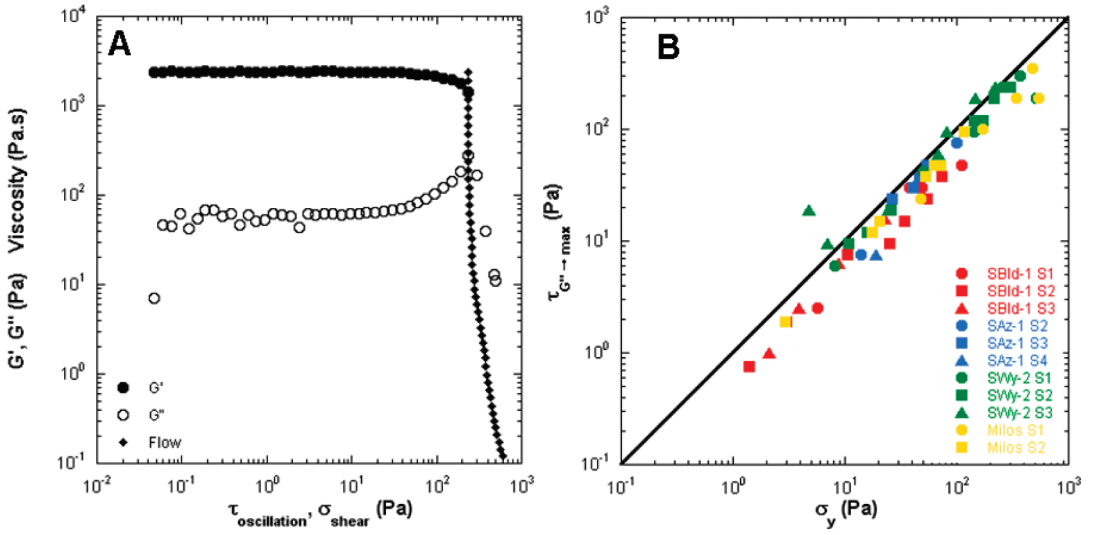

Figure 7. (A) Comparison between oscillation stress and flow curves (SWy-2 S2, IS = 10^{-5} M·L^{-1}, ϕ_{sph} = 4.07). (B) Variation of the yield stress σ_y with the critical oscillation stress $\tau_{G''\rightarrow max}$ taken at the maximum of G'' for various size-selected suspensions of beidellite and montmorillonites at an ionic strength of 10^{-5} M·L^{-1}.

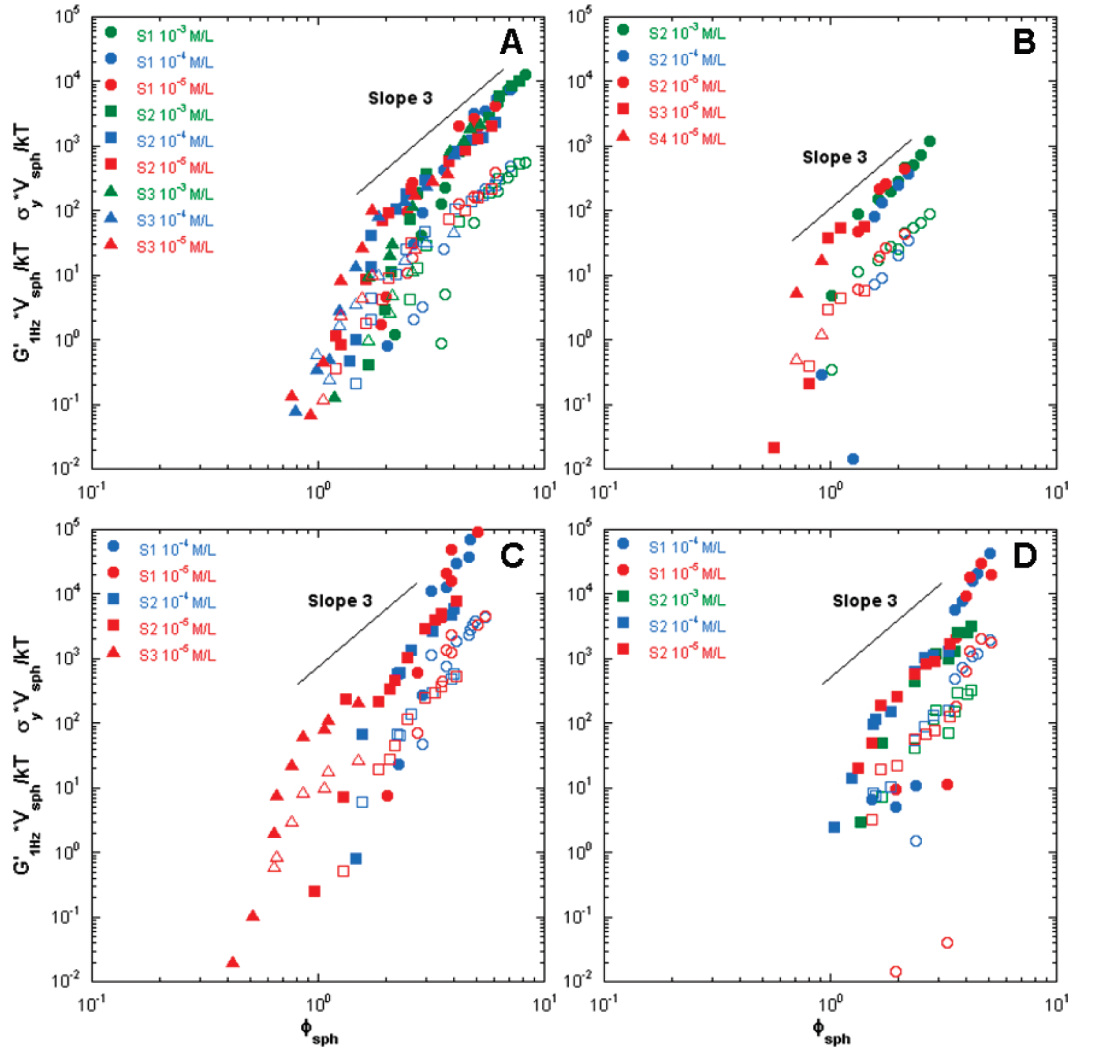

Figure 8. Variation of the normalized elasticity $G'_{1\ Hz}$ (filled symbols) and yield stress σ_y (open symbols) with the spherical volume fraction at various ionic strengths for (A) SBId-1, (B) SAz-1, (C) SWy-2, and (D) Milos.

dx.doi.org/10.1021/la2001267 |*Langmuir* 2011, 27, 7806–7819

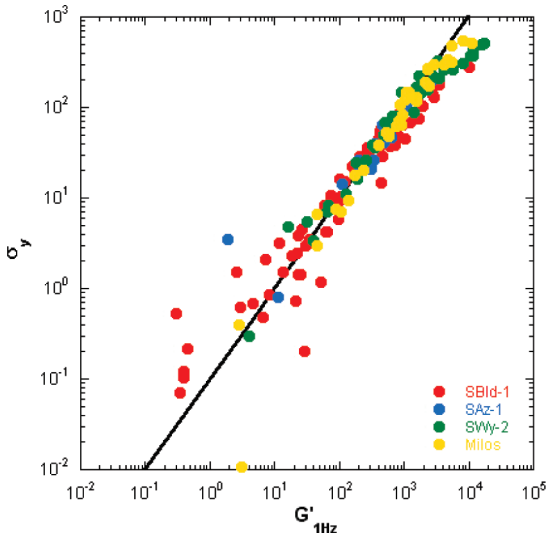

Figure 9. Variation of elasticity $G'_{1\ Hz}$ with yield stress σ_y for aqueous size-selected beidellite and montmorillonite suspensions at various ionic strengths. The solid black line corresponds to eq 6 with $\gamma_c = 0.1$.

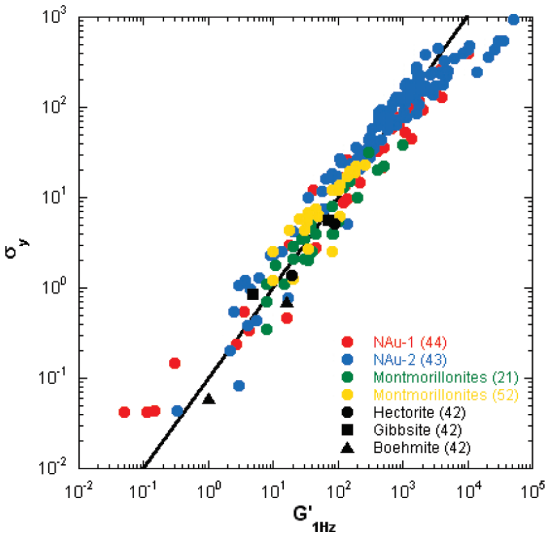

Figure 10. Variation of the elasticity $G'_{1\ Hz}$ with the yield stress σ_y for various colloidal suspensions obtained from the literature. Nontronites NAu-1 and NAu-2,[43,44] montmorillonites extracted from different bentonites,[21,52] and hectorite, gibbsite, and boehmite[42] suspensions. The solid black line corresponds to eq 6 with $\gamma_c = 0.1$.

whose diameter $\langle D \rangle$ is that of the particle (Table 2) and divided by kT so as to yield a dimensionless number.

For all clays, both G' (filled symbols) and σ_y (open symbols) appear to follow the same master curve irrespective of the size and ionic strength. For spherical volume fractions ϕ_{sph} significantly higher than 1, a power law with an exponent of 3 appears to describe both the elasticity and yield stress adequately. This is less the case for the highest size fractions of Wyoming and Milos montmorillonites where exponents between 3 and 3.5 are obtained, which can be related to the high polydispersity of these suspensions (Table 2). It also appears that for all volume fractions investigated the elasticity values are systematically higher than the yield stress values. The relationship between both parameters is plotted in Figure 9 for beidellite and montmorillonites.

As expected, the yield stress dependence is linear and can be written as

$$\sigma_y = G'\gamma_c \qquad (6)$$

with γ_c is the critical strain of the suspension, which is close to 0.1, in agreement with the results presented in Figure 4. The relationship is slightly less convincing on the high and low regions of the graph, where measurements are less accurate. This relationship seems to be independent of size, ionic strength, and nature of the clay. To analyze if such behavior is generic, we have plotted in Figure 10 values obtained previously by us for nontronites[43,44] as well as data obtained by several authors on different montmorillonite[21,52] and hectorite[42] suspensions or on other mineral colloidal dispersions of various shapes.[42]

All data for anisometric particles are well described using a critical strain of 0.1, which suggests that this behavior may be generic. Similar relationships have also been obtained for systems of spherical particles,[75,77−79] but data on spheres appear to exhibit a wider range of γ_c values extending between 0.1 and 1.0.

The influence of the nature of the clay on the rheological properties of the gels can be analyzed by plotting the normalized elasticity and yield stress as a function of the reduced spherical volume fraction defined as $(\phi_{sph} - \phi_{sph\ sol-gel})$, with $\phi_{sph\ sol-gel}$ being the spherical volume fraction corresponding to the sol−gel transition (Table 4). Figure 11 presents this normalization applied to gels of beidellite and montmorillonites with equivalent average diameters (∼200 nm) at various ionic strengths.

Using such a treatment, the elasticity and yield stress exhibit a close to $(\phi_{sph} - \phi_{sph\ sol-gel})^2$ dependence, similar to what was observed for montmorillonite,[33,41] Nau2 nontronite,[43] NAu-1 nontronite,[44] and laponite.[35−38] In addition, the scaling exponent does not depend on the ionic strength, in contrast to the results reported for attractive colloidal systems[54,80−83] that display exponent values of around 4 that strongly depend on the ionic strength. This power law then appears to be characteristic of all swelling clay minerals regardless of the presence of an isotropic to nematic (I/N) transition before the sol−gel transition.

Still, the nature of the clay influences the gel elasticity. Indeed, G' increases in the order SBId-1 < Milos ≈ SAz-1 < SWy-2. Such a sequence is the same as that derived from osmotic stress measurements or analyses of the structure factors of the suspensions. (See Figure 13 of ref 45.) It then appears that more repulsive clay systems display a lower elasticity than the less repulsive ones, a feature that may provide some key to predicting the rheological properties of gels of swelling clay minerals better.

Sol−Gel Transition. In this section, we will try to understand why in all swelling clays studied so far an increase in the average diameter of the clay platelets retards the sol−gel transition. At low volume fractions, individual particles are randomly oriented in the suspension and can freely rotate because of Brownian motion (Figure 12A). The spherical volume fraction ϕ_{sph} calculated from eq 1 corresponds to the hydrodynamic volume trapped by a freely rotating particle.

The sol−gel transition occurs when both rotational and translational jamming appear because of the hydrodynamic trapping of the entire free volume corresponding to $\phi_{sph} = 1$.[69]

Figure 13A presents the evolution of the spherical volume fraction corresponding to the sol−gel transition as a function of the average particle diameter. Independently of the nature of the clay, a clear dependence is observed, with higher size fractions

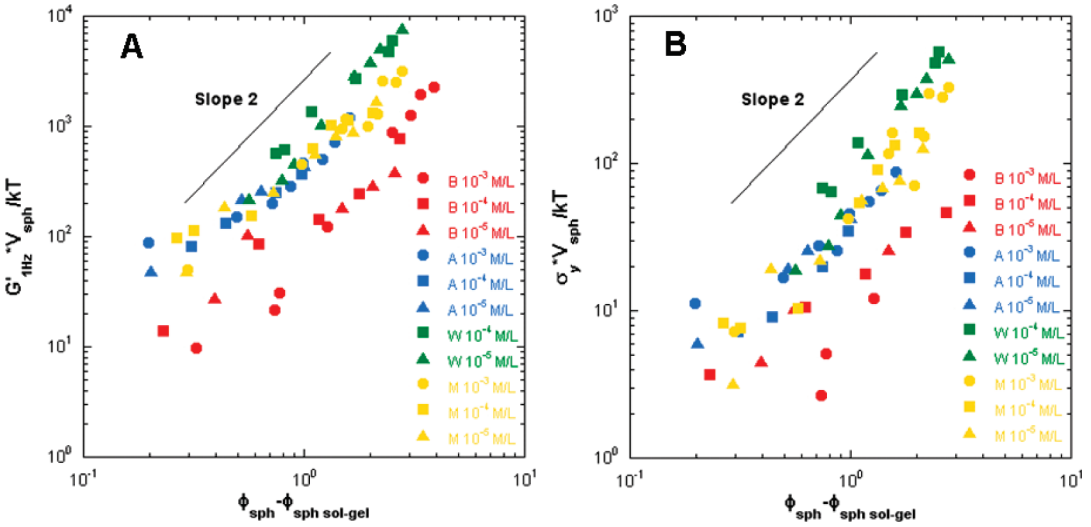

Figure 11. Variation of (A) the normalized elasticity $G'_{1\ Hz}$ and (B) the normalized yield stress with a reduced spherical volume fraction at various ionic strengths for smectite suspensions with an average diameter of 200 nm. B, SBId-1 S3; A, SAz-1 S2; W, SWy-2 S2; M, Milos S2.

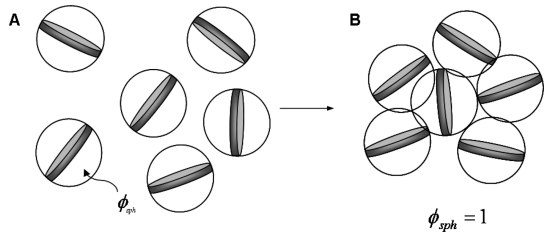

Figure 12. Schematic view of the sol−gel transition for individual disk-shaped particles. ϕ_{sph} corresponds to the hydrodynamic volume described by eq 1.

leading to retarded sol−gel transitions. To understand the influence of particle size on the sol−gel transition better, the values of the spherical volume fraction corresponding to the sol−gel transition $\phi_{sph\ sol-gel}$ have been converted to a density N that, for disks, can be written as

$$\phi = \frac{\pi}{4} N \langle D \rangle^2 t \tag{7}$$

with ϕ being the volume fraction of particles and $\langle D \rangle$ and t being the average diameter and thickness of the particle deduced from TEM and SAXS experiments, respectively. Combining eqs 1 and 7, N can be written as

$$N = \frac{6}{\pi} \frac{\phi_{sph}}{\langle D \rangle^3} \tag{8}$$

Using the values of Tables 2 and 4, we have represented in Figure 13B the evolution with average diameter of the number density corresponding to the sol−gel transition for beidellite and montmorillonite suspensions.

It appears that the number density at the sol−gel transition does not exhibit a −3 power law dependence on the average diameter, which suggests that the sol−gel transition might involve the association of particles rather than individual ones, a conclusion already derived from previous measurements on SWy-2 montmorillonites[41] and nontronites.[43,44]

The nature of such an association of particles and its dependence on size can be understood using a very simplified view based on the statistical hydrodynamic trapping of a particle by another one. Such a view follows similar thought lines as those used in a different context to explain the shear thickening of colloidal dispersions on the basis of the formation of hydroclusters.[84,85] Such hydrodynamic trapping has also been invoked to explain the rheological features associated with the breaking of colloidal gels[86,87]

For low volume fractions, particles rotate randomly in the suspension (Figure 14A). Upon translation, a particle might hydrodynamically trap another one in its neighborhood. The pair thus formed can rotate together in a short period of time (Figure 14B). Then, the two particles dissociate and can again trap other particles (Figure 14C). According to such a view, the associated spherical volume fraction of the two particles ϕ'_{sph} is smaller than the sum of the spherical volume fraction, as $\phi'_{sph} < \phi_{1\ sph} + \phi_{2\ sph}$. This statistical hydrodynamic trapping mainly depends on the rotational and translational Brownian diffusion times, noted as $t_{B\ rot}$ and $t_{B\ trans}$, respectively. In suspensions of disk-shaped particles, both characteristic times scale as[40,74]

$$t_B \approx \frac{3}{16} \frac{k_B T}{\eta D} \tag{9}$$

where η_f is the viscosity of the suspending medium, k_B is the Boltzmann constant, and T is the absolute temperature. An effect can then occur if the characteristic time corresponding to trapping, t_{trap}, is comparable to the residence time of a particle in the vicinity of another one. Obviously, such a situation is unlikely for small size fractions where all particles move very quickly. In contrast, with increasing average diameter, such associations become statistically more frequent.

To assess such an assumption, it is necessary to analyze regions where the hydrodynamic effects are negligible (i.e., in the low shear limit). By applying Quemada's model,[74−76] the viscosity at low shear stress can be expressed as

$$\frac{\eta_0}{\eta_f} = \left(1 - \frac{\phi'_{sph}}{\phi^*_{sph}}\right)^{-2} \quad \text{with} \quad \begin{matrix} \phi'_{sph} = \alpha \phi_{sph} \\ \phi^*_{sph} = 1 \end{matrix} \tag{10}$$

dx.doi.org/10.1021/la2001267 |Langmuir 2011, 27, 7806–7819

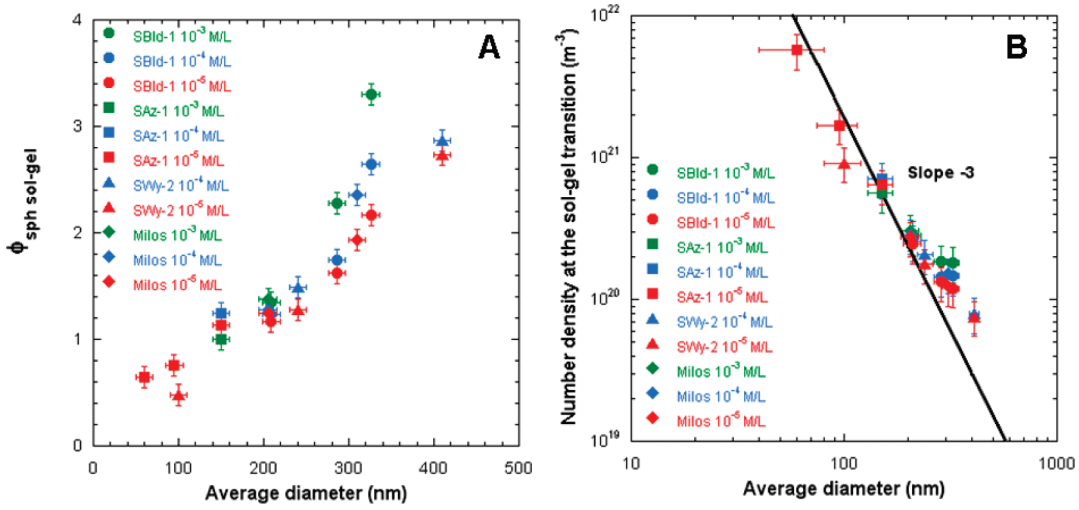

Figure 13. Variation with the average diameter of the spherical volume fraction (A) and the number density (B) corresponding to the sol−gel transition at different ionic strengths for various size fractions of beidellite and montmorillonite suspensions. The solid black line corresponds to eq 8 with $\phi_{sph} = 1$.

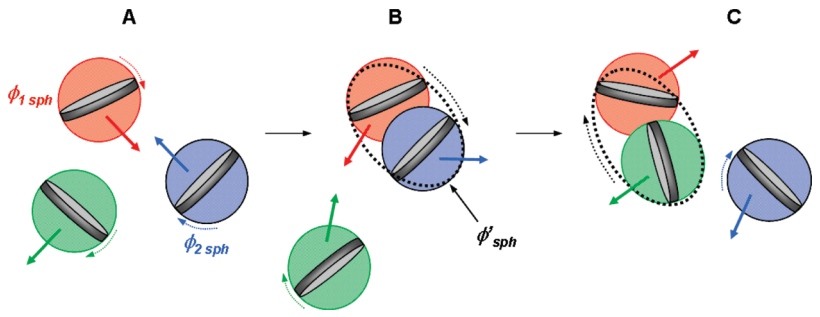

Figure 14. Schematic view of the statistical hydrodynamic trapping and the associated spherical volume fraction ϕ'_{sph}. (See the text.)

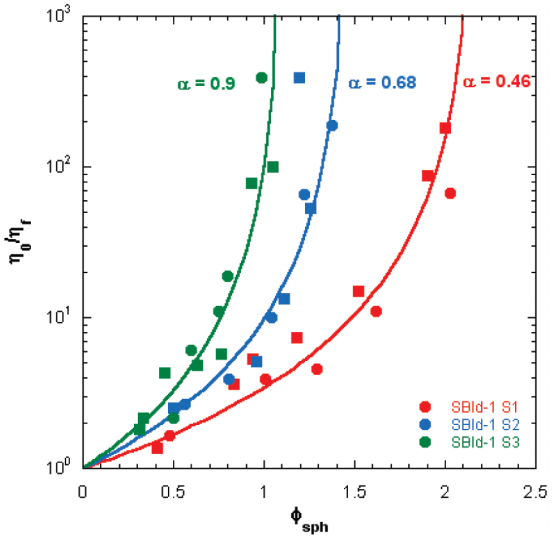

Figure 15. Evolution of the zero shear viscosity with the spherical volume fraction ϕ_{sph} for the three size fractions of beidellite suspensions: red, size 1; blue, size 2; green, size 3. Circles: IS = 10^{-4} M·L^{-1}. Squares: IS = 10^{-5} M·L^{-1}. The solid lines correspond to eq 10.

where α is a corrective parameter describing statistical hydrodynamic trapping. For freely rotating individual particles, α =1. For high size fractions, where particles can move together (Figure 16), α < 1. Figure 15 displays the evolution of η_0/η_f for the three size fractions of beidellite at ionic strengths of 10^{-4} and 10^{-5} M·L^{-1}. The curves shift toward higher spherical volume fractions with increasing size. Their shape can be convincingly modeled using decreasing α values for increasing sizes, in agreement with the proposed approach.

Figure 16 presents the evolution with average diameter of α for all of the clay samples investigated in the present study. Points obtained at an ionic strength of 10^{-3} M·L^{-1} are located slightly below the others. This can be related to the lowering of repulsive interactions, which favors trapping and consequently decreases α.

Still, a common trend appears for all samples. α can then in a first approach be expressed as

$$\alpha \equiv \frac{1}{\left(\frac{\langle D \rangle}{L}\right)^3 + 1} \qquad (11)$$

In a crude approximation, α can be considered to be inversely proportional to the Brownian diffusion time. This latter quantity depends on the cube of the average diameter (eq 9). For very small particles (i.e., when $D \rightarrow 0$), α must be close to 1, according to its definition. To obtain an adimensional number, it is also necessary to introduce a characteristic length L. The adjustment of L to data displayed in Figure 16 yields L = 330 nm. It must be pointed out that the values obtained for the two smallest sizes of

dx.doi.org/10.1021/la2001267 |*Langmuir* 2011, 27, 7806–7819

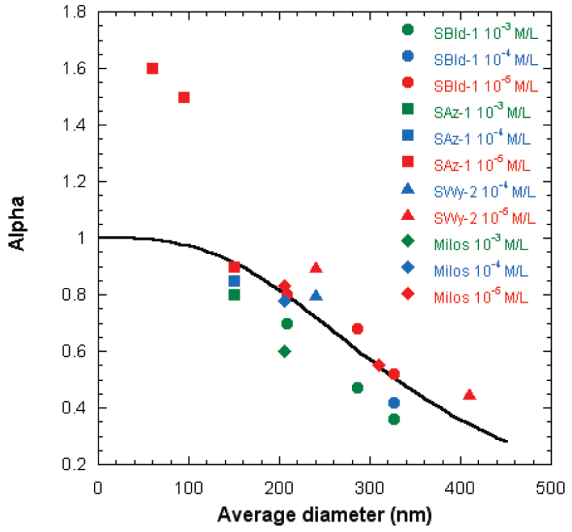

Figure 16. Variation of the α parameter with average diameter. The solid black line corresponds to eq 11 with L = 330 nm.

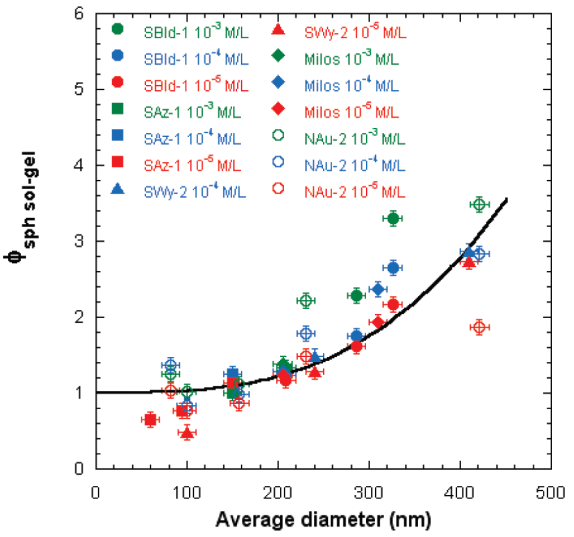

Figure 17. Variation of the spherical volume fraction corresponding to the sol−gel transition $\phi_{sph\ sol-gel}$ with the average diameter of beidellite, montmorillonite, and nontronite[43] particles at various ionic strengths. The solid black line represents $1/\alpha(D)$. (See the text.)

SAz-1 montmorillonite for an ionic strength of 10^{-5} M·L^{-1} are greater than 1, which can be assigned to the fact that the average particle diameter is of the same order of magnitude as the Debye length. Figure 17 presents the same data as that of Figure 13A, with added data previously obtained for Nau2 nontronite.[43] We have also reported in Figure 17 the evolution of $1/\alpha(D)$ derived from eq 11.

It appears that, except for some of the values obtained at an ionic strength of 10^{-3} M·L^{-1}, satisfactory agreement is obtained between experimental and modeled values. The very simplified approach proposed in this article and based on the hydrodynamic trapping of particles therefore captures most features of the sol−gel transition in all swelling clay minerals and could then explain why the largest particles form gels at higher volume fractions than the smallest one.

High Shear Flow Properties. At infinite shear viscosity η_∞, hydrodynamic effects dominate Brownian motion, which provides information in terms of particle alignment in the flow as already described.[40,43] New development techniques can also probe particle orientation under flow.[88,89] Figure 18 presents the variation of infinite shear viscosity obtained from eq 3 plotted as a function of the spherical volume fraction for the three size fractions of beidellite (Figure 18A) and for all clays with equivalent average diameters (Figure 18B).

Depending on the clay concentration, two different regimes can systematically be observed. At a low spherical volume fraction, all data points fall on the same master curve. At a higher spherical volume fraction, all of the curves exhibit a pseudoplateau. The viscosity values at the plateau are always low, less than 1 order of magnitude higher than the viscosity of water. This illustrates the strongly shear-thinning behavior of clay suspensions. Such a feature can be understood by assuming that particles under shear align along velocity streamlines. Under such a condition, their hydrodynamic drag is strongly reduced, and in the case of close to perfect orientation, the addition of more aligned particles has only a small effect on viscosity, which explains the occurrence of a pseudoplateau in the evolution of infinite shear viscosity with volume fraction. The alignment of particles with their normal perpendicular to the velocity streamlines has recently been confirmed by RheoSAXS experiments.[90,91]

Figure 18A clearly shows that the viscosity value at the plateau decreases with decreasing size, evidencing a better orientation in the flow of smaller particles as already shown[43,44] and confirmed by an ongoing rheoSAXS investigation.[90,91] In addition, for a given size, an increase in ionic strength displaces the plateau toward higher viscosity values. It then appears that the higher the electrostatic repulsion between clay platelets, the better they align parallel to each other in the flow.

In that context, the differences observed in Figure 18B between the different clay samples are indicative of significant variations in electrostatic repulsions. It is particularly striking that the repulsion order thus deduced is exactly the same as that deduced from elasticity (Figure 11A) and yield stress (Figure 11B) measurements. Such macroscopic properties at rest and under high shear flow are also perfectly correlated to the microscopic organization at rest, as deduced from the evolution of the clay nature of the structure factor of clay suspensions.[45] In the limit of large Peclet numbers $\gg$1, hydrodynamics effects dominate Brownian motion. Therefore, the discrepancy between particles is induced only by repulsive electrostatic interactions.

CONCLUSION AND PERSPECTIVES

We have investigated in depth the rheological behavior of various size-selected natural clays in aqueous suspensions, revealing that, in such systems, the viscoelastic properties are closely related to repulsive electrostatic interactions between platelets. Macroscopic mechanical properties are also dependent on the charge location in the clay structure. Indeed, both the yield stress and elasticity follow trends similar to those established in the first part of this series of papers,[45] and significantly decrease with increasing repulsive electrostatic interactions. This is particularly obvious in the case of tetrahedrally substituted beidellite. Though regularly confirmed, this strong difference between octahedrally and tetrahedrally substituted clays remains unclear and clearly deserves further experimental and theoretical investigation. Notwithstanding, this work also provides new insights into the size dependence of the sol−gel transitions. Using the

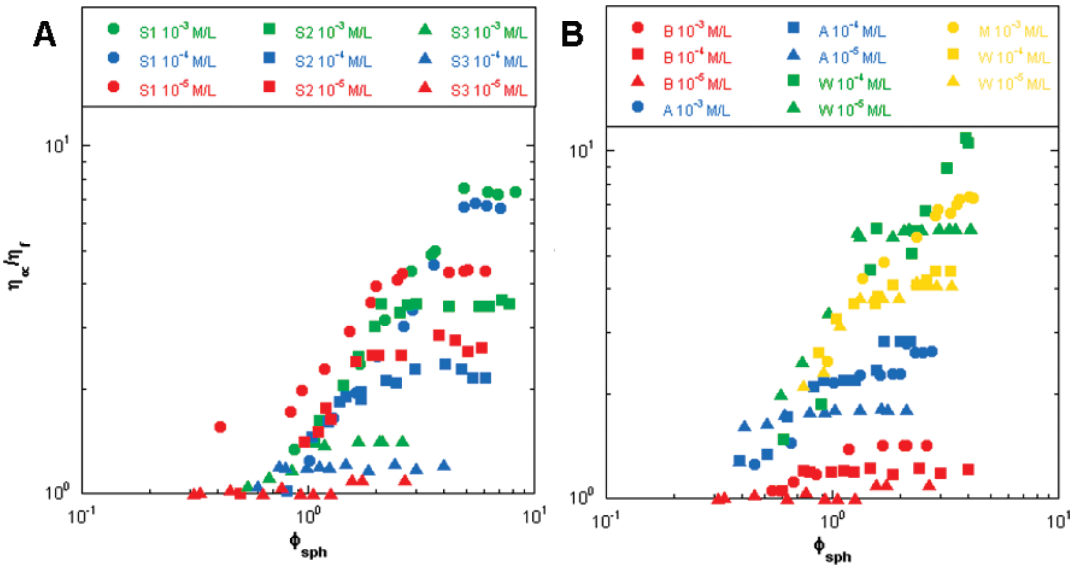

Figure 18. Variation of the infinite shear viscosity as a function of the spherical volume fraction. (A) SBId-1 and (B) smectites suspensions with an average diameter of 200 nm. B, SBId-1 S3; A, SAz-1 S2; W, SWy-2 S2; and M, Milos S2.

very simplified approach proposed in this article, we assigned this dependence to the statistically hydrodynamic trapping of platelets resulting in a transient lowering of the volume fraction. Still, it must be pointed out that such an explanation holds only if Brownian motion dominates other interaction forces.

■ ASSOCIATED CONTENT

Supporting Information. Additional oscillation frequency and stress measurements. This material is available free of charge via the Internet at http://pubs.acs.org.

■ AUTHOR INFORMATION

Corresponding Author

*E-mail: erwan.paineau@ensg.inpl-nancy.fr; christophe.baravian@ensem.inpl-nancy.fr.

■ ACKNOWLEDGMENT

We gratefully acknowledge the French ANR for financial support under the ANR-07-BLANC-0194 program. We also thank one of the reviewers for bringing to our attention the concept of hydroclusters.

■ REFERENCES

(1) Rice, P. M. *J. Archaeol. Method Theory* **1999**, *6*, 1–54.
(2) Odom, I. E. *Phil. Trans. R. Soc. London, Sect. A* **1984**, *311*, 391–409.
(3) Murray, H. H. *Appl. Clay Sci.* **2000**, *17*, 207–221.
(4) Freundlich, H. *Kolloid-Z.* **1928**, *46*, 289–299.
(5) Ross, C. S.; Shannon, E. V. *J. Am. Ceram. Soc.* **1926**, *9*, 77–96.
(6) Broughton, G.; Squires, L. *J. Phys. Chem.* **1936**, *40*, 1041–1053.
(7) Hauser, E. A.; Reed, C. E. *J. Phys. Chem.* **1937**, *41*, 911–934.
(8) Langmuir, I. *J. Chem. Phys.* **1938**, *6*, 873–896.
(9) Van Olphen, H. *Discuss. Faraday Soc.* **1951**, *11*, 82–84.
(10) Van Olphen, H. *Clays Clay Miner.* **1956**, *4*, 204–224.
(11) Van Olphen, H. *J. Colloid Sci.* **1964**, *19*, 313–322.
(12) Lockhart, N. C. *J. Colloid Interface Sci.* **1980**, *74*, 509–519.
(13) Neumann, B. S. *Rheol. Acta* **1965**, *4*, 250–255.
(14) Neumann, B. S.; Sansom, K. G. *Clay Miner.* **1971**, *9*, 231–243.
(15) Khandal, R. K.; Tadros, Th. F. *J. Colloid Interface Sci.* **1988**, *125*, 122–128.
(16) Keren, R.; Shainberg, I.; Klein, E. *Soil Sci. Soc. Am. J.* **1988**, *52*, 76–80.
(17) Keren, R. *Soil Sci. Soc. Am. J.* **1988**, *52*, 924–928.
(18) Miano, F.; Rabaioli, M. R. *Colloids Surf., A* **1994**, *84*, 229–237.
(19) Willenbacher, N. *J. Colloid Interface Sci.* **1996**, *182*, 501–510.
(20) Durán, J. D. G.; Ramos-Tejada, M. M.; Arroyo, F. J.; González-Caballero, F. *J. Colloid Interface Sci.* **2000**, *229*, 107–117.
(21) Ramos-Tejada, M. M.; Arroyo, F. J.; Perea, R.; Durán, J. D. G. *J. Colloid Interface Sci.* **2001**, *235*, 251–259.
(22) M'Ewen, M. B.; Mould, D. L. *Nature* **1950**, *166*, 437–438.
(23) M'Ewen, M. B.; Pratt, M. I. *Trans. Faraday Soc.* **1957**, *53*, 535–547.
(24) Rand, B.; Pekenć, E.; Goodwin, J. W.; Smith, R. W. *J. Chem. Soc., Faraday Trans.* **1980**, *76*, 225–235.
(25) Vali, H.; Bachmann, L. *J. Colloid Interface Sci.* **1988**, *126*, 278–291.
(26) Heller, H.; Keren, R. *Clays Clay Miner.* **2001**, *49*, 286–291.
(27) Tombácz, E.; Szekeres, M. *Appl. Clay Sci.* **2004**, *27*, 75–94.
(28) Weiss, A.; Frank, R. Z. *Naturforsch* **1961**, *16*, 141–142.
(29) Brandenburg, U.; Lagaly, G. *Appl. Clay Sci.* **1988**, *3*, 263–279.
(30) Lagaly, G. *Appl. Clay Sci.* **1989**, *4*, 105–123.
(31) Norrish, K. *Discuss. Faraday Soc.* **1954**, *18*, 120–134.
(32) Hauser, E. A. *Chem. Rev.* **1945**, *40*, 287–321.
(33) Callaghan, I. C.; Ottewill, R. H. *Faraday Discuss.* **1974**, *57*, 110–118.
(34) Lubetkin, S. D.; Middleton, S. R.; Ottewill, R. H. *Philos. Trans. R. Soc. London, Sect. A* **1984**, *311*, 353–368.
(35) Ramsay, J. D. F. *J. Colloid Interface Sci.* **1986**, *109*, 441–447.
(36) Mourchid, A.; Delville, A.; Levitz, P. *Faraday Discuss.* **1995**, *101*, 275–285.
(37) Mourchid, A.; Delville, A.; Lambard, J.; Lécolier, E.; Levitz, P. *Langmuir* **1995**, *111*, 1942–1950.
(38) Mourchid, A.; Lécolier, E.; Van Damme, H.; Levitz, P. *Langmuir* **1998**, *14*, 4718–4723.
(39) Adachi, Y.; Nakaishi, K.; Tamaki, M. *J. Colloid Interface Sci.* **1998**, *198*, 100–105.
(40) Baravian, C.; Vantelon, D.; Thomas, F. *Langmuir* **2003**, *19*, 8109–8114.
(41) Michot, L. J.; Bihannic, I.; Porsch, K.; Maddi, S.; Baravian, C.; Mougel, J.; Levitz, P. *Langmuir* **2004**, *20*, 10829–10837.

(42) Ten Brinke, A. J. W.; Bailey, L.; Lekkerkerker, H. N. W.; Maitland, G. C. *Soft Matter* **2007**, *3*, 1145–1162.
(43) Michot, L. J.; Baravian, C.; Bihannic, I.; Maddi, S.; Moyne, C.; Duval, J. F. L.; Levitz, P.; Davidson, P. *Langmuir* **2009**, *25*, 127–139.
(44) Michot, L. J.; Paineau, E.; Bihannic, I.; Maddi, S.; Duval, J. F. L.; Baravian, C.; Davidson, P.; Levitz, P. *Clay Miner.*, accepted for publication.
(45) Paineau, E.; Bihannic, I.; Baravian, C.; Philippe, A. M.; Davidson, P.; Levitz, P.; Funari, S. S.; Rochas, C.; Michot, L. J. *Langmuir* **2011**, *27*, 5562–5573.
(46) Heath, D.; Tadros, Th. F. *J. Colloid Interface Sci.* **1983**, *93*, 307–319.
(47) Sohm, R.; Tadros, Th. F. *J. Colloid Interface Sci.* **1989**, *132*, 62–71.
(48) Schmidt, C. U.; Lagaly, G. *Clay Miner.* **1999**, *34*, 447–458.
(49) (a) Permien, T.; Lagaly, G. *Clay Miner.* **1994**, *29*, 751–760. (B) Permien, T.; Lagaly, G. *Clay Miner.* **1994**, *29*, 761–766.
(50) Lott, M. P.; Williams, D. J. A.; Williams, P. R. *Colloid Polym. Sci.* **1996**, *274*, 43–48.
(51) Benna, M.; Kbir-Ariguib, N.; Magnin, A.; Bergaya, F. *J. Colloid Interface Sci.* **1999**, *218*, 442–455.
(52) Abend, S.; Lagaly, G. *Appl. Clay Sci.* **2000**, *16*, 201–227.
(53) Pignon, F.; Piau, J. M.; Magnin, A. *Phys. Rev. Lett.* **1996**, *76*, 4857–4860.
(54) Martin, C.; Pignon, F.; Piau, J. M.; Magnin, A.; Lindner, P.; Cabane, B. *Phys. Rev. E* **2002**, *66*, 021401.
(55) Benna-Zayani, M.; Mgaidi, A.; Stambouli, M.; Kbir-Ariguib, N.; Trabelsi-Ayadi, M.; Grossiord, J. L. *Appl. Clay Sci.* **2009**, *46*, 260–264.
(56) Cocard, S.; Tassin, J. F.; Nicolai, T. *J. Rheol.* **2000**, *44*, 585–594.
(57) Shalkevich, A.; Stradner, A.; Bhat, S. K.; Muller, F.; Schurtenberger, P. *Langmuir* **2007**, *23*, 3570–3580.
(58) Michot, L. J.; Bihannic, I.; Maddi, S.; Funari, S. S.; Baravian, C.; Levitz, P.; Davidson, P. *Proc. Natl. Acad. Sci. U.S.A* **2006**, *44*, 16101–16104.
(59) Michot, L. J.; Bihannic, I.; Maddi, S.; Baravian, C.; Levitz, P.; Davidson, P. *Langmuir* **2008**, *24*, 3127–3139.
(60) Paineau, E.; Antonova, K.; Baravian, C.; Bihannic, I.; Davidson, P.; Dozov, I.; Impéror-Clerc, M.; Levitz, P.; Madsen, A.; Meneau, F.; Michot, L. J. *J. Phys. Chem. B* **2009**, *113*, 15858–15869.
(61) Hemmen, H.; Ringdal, N. I.; De Azevedo, E. N.; Engelsberg, M.; Hansen, E. L.; Méheust, Y.; Fossum, J. O.; Knudsen, K. D. *Langmuir* **2009**, *25*, 12507–12515.
(62) Miyamoto, N.; Iijima, H.; Ohkubo, H.; Yamauchi, Y. *Chem. Commun.* **2010**, *46*, 4166–4168.
(63) Boek, E. S.; Coveney, P. V.; Lekkerkerker, H. N. W.; van der Schoot, P. *Phys. Rev. E* **1997**, *55*, 3124–3133.
(64) Zhang, Z.; Krishna, N.; Lettinga, M. P.; Vermant, J.; Grelet, E. *Langmuir* **2009**, *25*, 2437–2442.
(65) Gruner, J. W. *Am. Mineral.* **1935**, *7*, 475–483.
(66) Vantelon, D.; Montarges-Pelletier, E.; Michot, L. J.; Briois, V.; Pelletier, M.; Thomas, F. *Phys. Chem. Miner.* **2003**, *30*, 44–53.
(67) Mourad, M. C. D.; Byelov, D. V.; Petukhov, A.; Matthijs de Winter, D. A.; Verkleij, A. J.; Lekkerkerker, H. N. W. *J. Phys. Chem. B* **2009**, *113*, 11604–11613.
(68) Baravian, C.; Benbelkacem, G.; Caton, F. *Rheol. Acta* **2007**, *46*, 577–581.
(69) Baravian, C.; Michot, L. J.; Paineau, E.; Bihannic, I.; Davidson, P.; Impéror-Clerc, M.; Belamie, E.; Levitz, P. *Europhys. Lett.* **2010**, *90*, 36005.
(70) Markgraf, W.; Horn, R.; Peth, S. *Soil Tillage Res.* **2006**, *91*, 1–14.
(71) Jogun, S.; Zukoski, C. F. *J. Rheol.* **1996**, *40*, 1211–1232.
(72) Jogun, S. M.; Zukoski, C. F. *J. Rheol.* **1999**, *43*, 847–871.
(73) Ramsay, J. D. F.; Daish, S. R.; Wright, C. J. *Farday Discuss. Chem. Soc.* **1978**, *65*, 65–75.
(74) Berli, C. L. A.; Quemada, D. *Langmuir* **2000**, *16*, 7968–7974.
(75) Berli, C. L. A.; Quemada, D. *Langmuir* **2000**, *16*, 10509–10514.
(76) Quemada, D.; Berli, C. *Adv. Colloid Interface Sci.* **2002**, *98*, 51–85.
(77) Buscall, R.; Goodwin, J. W.; Hawkins, M. W.; Ottewill, R. H. *J. Chem. Soc., Faraday Trans.* **1982**, *78*, 2873–2887.
(78) Chen, L. B.; Zukoski, C. F. *J. Chem. Soc., Faraday Trans* **1990**, *86*, 2629–2639.
(79) Fagan, M. E.; Zukoski, C. F. *J. Rheol.* **1997**, *41*, 373–397.
(80) Tadros, Th.F. *Adv. Colloid Interface Sci.* **1996**, *68*, 97–200.
(81) Trappe, V.; Prasad, V.; Cipelletti, L.; Segre, P. N.; Weitz, D. A. *Nature* **2001**, *411*, 772–775.
(82) Saint-Michel, F.; Pignon, F.; Magnin, A. *J. Colloid Interface Sci.* **2003**, *267*, 314–319.
(83) Russel, W. B.; Saville, D. A.; Schowalter, W. R. *Colloidal Dispersions*, 2nd ed.; Cambridge University Press: Cambridge, U.K., 1991.
(84) Bender, J. W.; Wagner, N. J. *J. Colloid Interface Sci.* **1995**, *172*, 171–184.
(85) Maranzano, B. J.; Wagner, N. J. *J. Chem. Phys.* **2002**, *117*, 10291–10302.
(86) Russel, W. B. *Powder Technol.* **1987**, *51*, 15–25.
(87) Vermant, J.; Solomon, M. J. *J. Phys.: Condens. Matter* **2005**, *17*, R187–R216.
(88) Mobuchon, C.; Carreau, P. J.; Heuzey, M. C.; Reddy, N. K.; Vermant, J. *J. Rheol.* **2009**, *53*, 517–538.
(89) Pujari, S.; Dougherty, L.; Mobuchon, C.; Carreau, P. J.; Heuzey, M. C.; Burghardt, W. R. *Rheol. Acta* **2011**, *50*, 3–16.
(90) Bihannic, I.; Baravian, C.; Duval, J. F. L.; Paineau, E.; Meneau, F.; Levitz, P.; De Silva, J. P.; Davidson, P.; Michot, L. J. *J. Phys. Chem. B* **2010**, *114*, 16347–16355.
(91) Philippe, A. M.; Baravian, C.; Impéror-Clerc, M.; De Silva, J.; Paineau, E.; Bihannic, I.; Davidson, P.; Meneau, F.; Levitz, P.; Michot, L. J. *J. Phys.: Condens Matter* **2011**, *23*, 194112